Project title: **NAtuRal instability of semiConductors thIn SOlid films for sensing and photonic applications (NARCISO)**
Grant Agreement: 828890
Call identifier: H2020-FETOPEN-2018-2020/H2020-FETOPEN-2018-2019-2020-01
Start Date of Project: 01/03/2019
Duration: 42 months

Deliverable D5.1– V1.0

Title: Parameterization of flow properties dependence on medium structure

Leader partner	UNIL
Author(s)	Pietro de Anna
Estimated delivery	28/02/2021
Actual delivery	
Revised version	
Work Package	WP4- Colloids and microbes transport and filtration
Tasks	4.2 – 4.3 – 4.4
Dissemination level	Public
Version	1.0

Contents

1. Introduction

We report on the achievement of colloidal transport through microfluidics chip representing relatively porous systems whose geometry is hyperuniform and it is characterized by size-distributed dead-end-pore able to trap mobile colloids. The impact of dead-end-pores (those that do not contribute to the overall fluid transfer) on solutes and suspensions has been investigated for decades but never completely unraveled: classical models simplify the transport description to a dual-system (mobile-immobile), the first characterized by fluid motion (advection), the latter by molecular diffusion. We investigate the role played by these dead-end-pores in a relatively homogeneous medium, printing via soft-lithography the geometries of de-wetted materials obtained by AMU.

2. Porous structure characterization

We used soft lithography to print the hyperuniform porous structure (see *figure 1 a* and *b*) chosen to represent the solid matrix of a porous material into a silicon wafer used as a mold for a PDMS microfluidics chip. A mask of irregular grain features characterized by a porosity of 0. and obtained from the solid-state dewetting process (image obtained from AMU), served as a template for the porous medium. We scaled the geometry in a way that the average pore-size is λ = 0.027 mm. The characterization of the pore space with the local pore-size and the segregation index, highlights the signature of two distinct pore features: Transferring-Pores (TP) and Dead-End-Pores (DEP). The pore size (λ) across the domain is homogeneously distributed: the value of the pore size ranges within a quite narrow set and it has a strong peak about the average pore size λ_m (see *figure 1 c*). We define the segregation index, that captures the dual feature of the matrix: it refers to the number *z* of individual grains surrounding an individual pore space (TP *z*: > 1 and DEP: *z* = 1). A grain is a black cluster in the geometry, in the experiment it corresponds to a solid impermeable obstacle. The dead-end-pores typically are elongated regions caving inside a singular grain in contrast to the transferring-pores (open channels) that are surrounded by multiple grains (see *figure 1 e*). We quantify the aspect ratio (Λ) as the DEP area to λ^2. For the studied medium, the distribution of such aspect ratio spans within [1,20] (see *figure 1 f*).

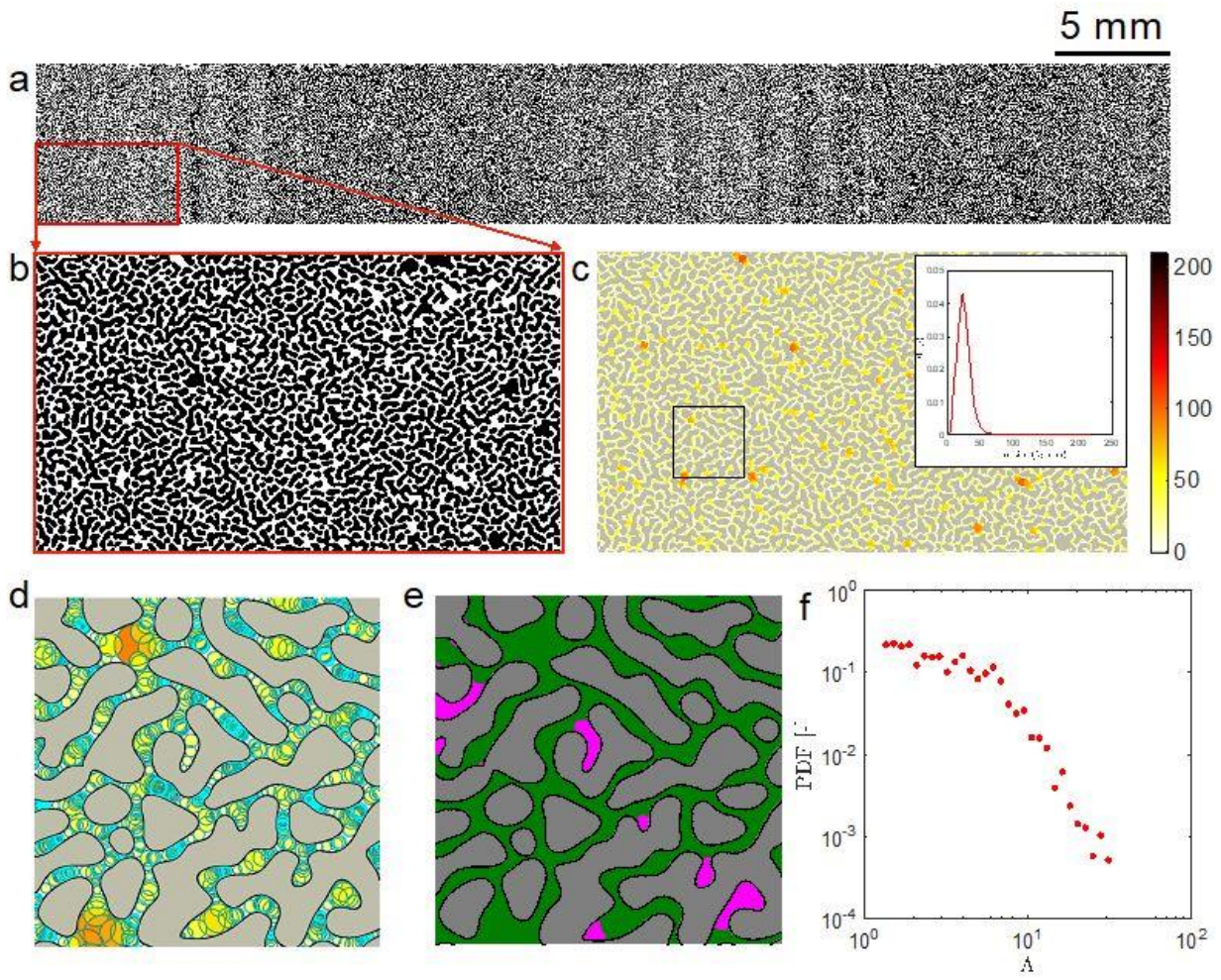

Figure 1 - a) Hyperuniform porous structure; b) close view; c) pore size characterization and (inset) pore size distribution; d) principle of maximum inscribed circle; e) Transferring-porePand Dead-End-Pore (DEP) characterization; f) DEP aspect-ratio distribution

3. Flow system and transport characterization

The printed microchannel (L = 51 mm x w = 7 mm x a = 0.083 mm) is slightly thicker than the average pore opening, λ (representative of many common geological structures, see *figure 2 a*). The narrow range of values for a/λ, about unity, yields a parabolic-like velocity profiles in both vertical and horizontal directions within pores, as verified by Particle Image Velocimetry (PIV). The effect of this heterogeneity is the emergence of a strong spatial correlation in the velocity field, in the form of fast flow pathways within the TPs and areas of fluid stagnation in the DEPs.

We investigate the impact of such medium structure on macroscopic transport using a neutrally buoyant, density matched, suspension of colloidal particles (0.5 μm polystyrene micro-spheres ρ = 1.05 g/mL in 1:1 milliQ - D_2O mixture) that initially saturates the porous system. Using the same strategy to inject a sharp front as in (Scheidweiler et al. JRSI 2020), a displacing solution with same density (1.05 g/mL), was withdrawn at a constant flow rate Q = 0.5 μL/min through the microfluidics

circuit eluting one pore volume (i.e. the volume of the entire porous channel) every 23.8 min, for 48 hours in total.

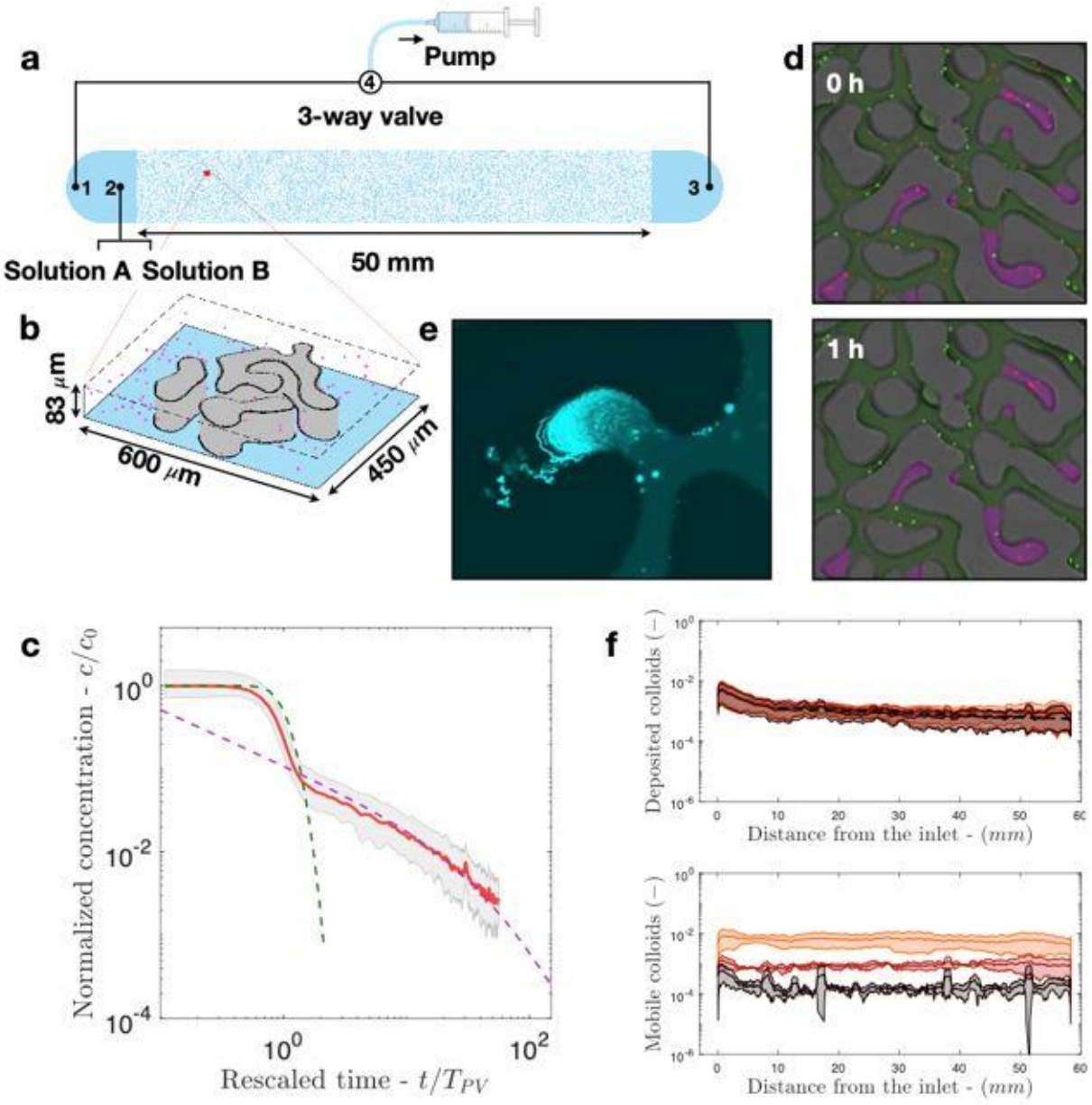

Figure 2. a) schematic of the experimental setup; b) schematic of a single dead-end-pore; c) measured colloids breackthrough curve (average and standard deviation over 3 replicates); d) two snapshots of mobile (red) and immobile (green) colloids within 0 and 1 h; f) deposition profile (top) and mobile-particles profile.

Time-lapse composite imaging coupled with fluorescence microscopy allowed us to count the number of effluent colloids near the outlet and compute their breakthrough curve (BTC). The latter is displayed in *figure 2 c* and shows two distinct transport regimes. The first one, limited to the elution of a few pore-volume (T_{PV}), is well captured by the classical advection-dispersion framework

(green dashed line in figure 2 *c*). At larger times ($t/T_{PV} > 1$), the BTC deviates from the exponential decay and gets a power law-like heavy tail, typical of so-called anomalous transport behavior.

We continuously monitored the spatial distribution of suspended colloids within the porous system by periodically collecting two composite images of the entire microfluidic channel (38 x 9 individual pictures) 7 times (0, 1, 4, 10, 16, 22 and 44 hours after injection), temporally separated by 60 s. The comparison of these consecutive images allows us to determine what particles are suspended and what particles got retained by the host solid structure. Figure 2 d shows a close view of a few pores just before the injection and 2 T_{PV} later: the number of immobile particles (green dots) does not increase with time, no filtration takes place, while the mobile particles (red dots), originally filling homogeneously the pore space (green shaded area), are depleted from the TPs while they still occupy the DEPs (magenta shaded area). In figure 2 *f* it is reported the spatial profile of the mobile particles that is homogeneously decaying throughout the porous system.

While it is common to assume that the fluid velocity within the DEPs is so small that it is negligible and does not play a role in the macroscopic transport, which is assumed to be fully dominated by molecular diffusion alone, we show the existence of a complex flow structure within each DEP that, coupled with molecular diffusion, controls the macroscopic BTC. In *figure 2 e* it is shown the superposition of 100 pictures of transported colloidal suspension: colloids move in the TP so fast that they do not leave any detectable signal of their passage; however, at the entrance of a DEP, where the velocity is smaller, it is visible a vortex characterized by closed trajectories. Moving within the inner part of the DEP the fluid velocity magnitude decays rapidly and molecular diffusion starts dominating individual tracks of random walkers are visible as short and tortuous segments.

Owing to experimental difficulties in resolving the multi-scale nature of such a flow field with a Particle Image Velocimetry (PIV) approach, in order to examine the flow structure within the DEPs we computed the velocity field inside a subsection of the primary porous matrix by solving the two-dimensional steady state incompressible Stokes flow equation using COMSOL Multiphysics. The domain of this numerical computation is approximately one-fifth in length (L = 11 mm) and the same in width (w = 7 mm), as that one used in the experiment. In *figure 3 a* it is shown the velocity field magnitude in a logarithmic scale (increasing velocity from light to dark). We discretized the flow domain using a physics based unstructured mesh with approximately 2.6 10^6 elements. We imposed no-slip boundary conditions at domain boundaries and a zero, reference, pressure at the outlet. We imposed a uniform flow rate of 0.5 μL/min, as in the experiment. The computational resolution is high enough to ensure a divergence free velocity field, as verified *a posteriori*. We further simulated the transport of $N = 10^5$ particles flowing with the computed velocity field and by molecular diffusion with $D_m = 10^{-6}$ mm^2/s, based on a Langevin equation.

In *figure 3 b* we report the BTC computed from arrival time distribution of the simulated tracks: it shows the same two regimes observed with our experimental setup. We investigate the initial position of the ''fast'' tracks that contribute to the early time regime and the ''slow'' ones contributing to the late time tailing, to highlight the driving mechanisms: the first are represented by green dots in the inset of *figure 3 a*, whereas the latter as red dots. It is clear that the late time scaling is due to the particles initially trapped within the DEPs and all particles not in DEPs get

washed-out from the medium before $t/T_{PV} = 2$. A close view of the velocity field magnitude around a DEP is shown in *figure 3 c*, in logarithmic color scale (for increasing value, from light to dark) superposed to few streamlines (in blue): the flow structure within a DEP is organized in a cascade of vortexes (closed trajectories) with velocity decaying while penetrating the DEP itself. In this scenario, only molecular diffusion can let particles escape from DEP, by jumping from a inner flow line to an outer one. This mechanism can be seen by plotting a single trajectory initiated within that DEP (*figure 3 d)*. The trajectory is color-coded (for increasing values, from dark to light) with the local Peclet number defined as $Pe = \lambda\, v_p / D_m$ where v_p is the local velocity of the tracked particle *p*. Initially, the particle transport is dominated by its molecular diffusion (dark color of the track) and as it approaches the outer vortex of the DEP it diffuses and also recirculates (Pe close to unity), and, then, it flows away (high Pe).

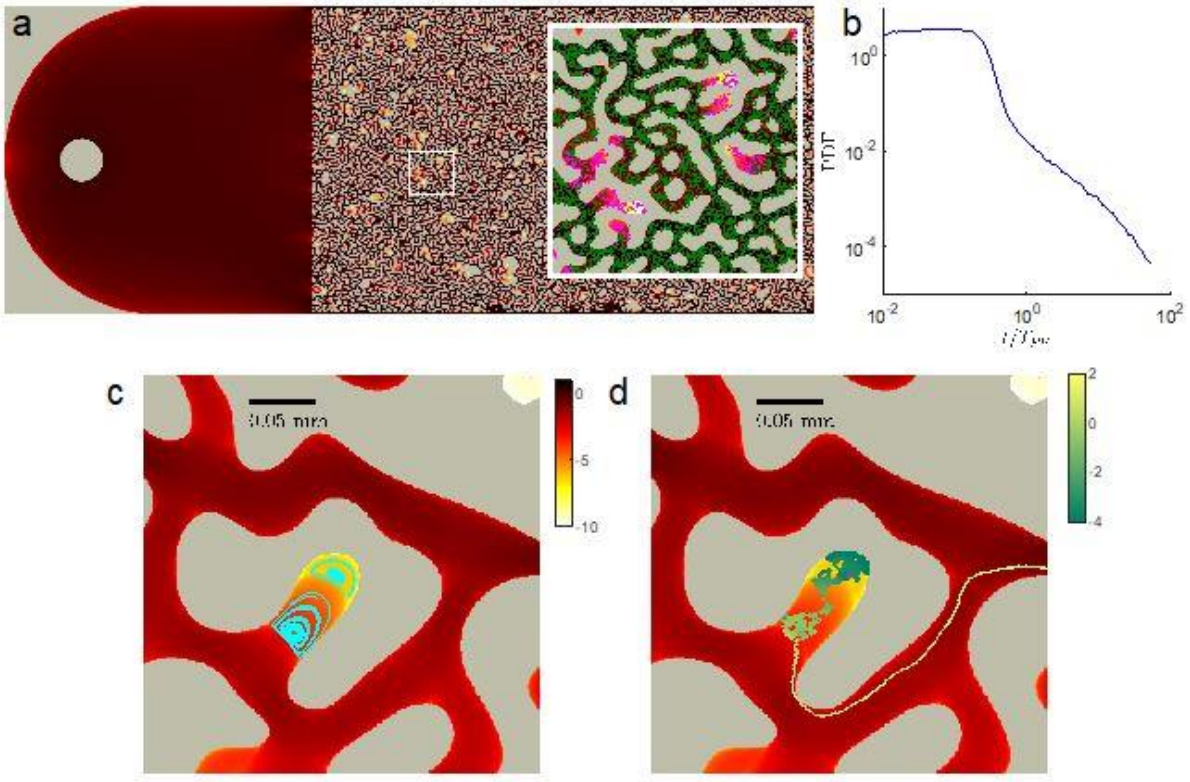

Figure 3 - a) simulation of the pore-scale flow field (Stokes equations solved); b) BTC from particle tracking simulations; c) detail fo the DEP flow structure; d) an individual trajectory leaving the DEP.

4. Modeling transport through hyperuniform porous structures

To understand how the two detected mechanisms, re-circulation within a vortex and jumps among flow-lines due to molecular diffusion, are coupled to control the late time BTC scaling, we model transport within a single DEP generalizing its geometry as a rectangular cavity connected to a free rectangular channel of side λ (same as the mean pore size) and different with-to-length aspect ratio $\Lambda = 1, 2, 4$ and 8. In *figure 4 a* it is shown the simulation result for the 3-dimensional case, $\Lambda = 4$: the flow structure is highlighted by the closed streamlines (continuous lines with different colors for

different *y*-plane location) associated to the vortexes of decaying intensity with depth. The trajectory of a particle initiated at the bottom of the DEP is shown as dots color-coded with the defined local Peclet number (in logarithmic scale), with increasing value from dark to light. The particle diffuses isotropically (Peclet number smaller than one) until it eventually gets to the upper part of the DEP, where its motion is given by the competition between advection along the top vortex streamlines and diffusion that promotes streamlines exchange (Peclet number close to unity) and it eventually leaves the DEP with the fast channel flow (Peclet number much higher than one).

Using the same numerical scheme adopted to simulate the transport through the hyperuniform porous geometry, we computed the trajectory of N = 10^5 particles originally homogeneously distributed within the DEP volume. In *figure 4 b* it is shown the BTC for different aspect-ratios Λ: for all cases it decays as the power law $t^{-2/3}$, which is significantly different from the scaling expected for diffusion alone, $t^{-1/2}$, with a late time exponential cut-off, in other words, a Γ-function. We understand the temporal scale of the cut-off as characteristic time of diffusion over the DEP depth $\tau_D = (\Lambda\lambda)^2/D$.

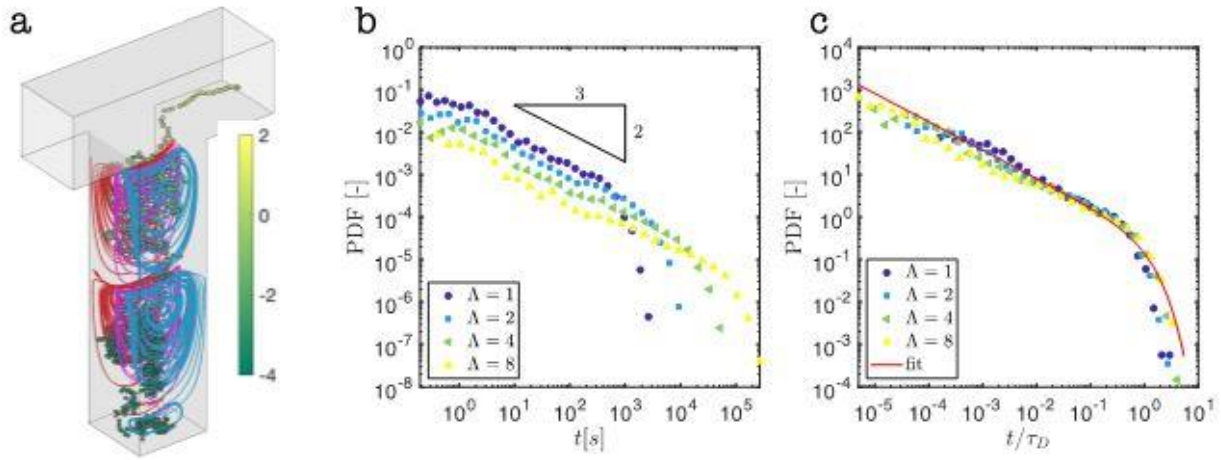

Figure 4 - a) Simulation of a 3D cavity flow as DEP model superposed to a few streamlines highlighting the vortex flow structure and a single trajectory; b) BTC of a single cavity for different aspect-ratio; c) same as b, with rescaled time.

In *figure 4 c* it is shown the BTC of the different aspect ratio Λ versus time re-scaled with τ_D: all BTCs collapse on the following Γ-distribution

$$f(t/\tau_D) = \frac{1}{\Gamma(\frac{2}{3})\,\tau_D^{1/3}} \left(\frac{t}{\tau_D}\right)^{-2/3} e^{-\frac{t}{\tau_D}}.$$

The characteristic temporal scaling of 2/3 is controlled by the combined effect of moving by advection along the closed streamlines of vortexes and jumping, by diffusion, among neighboring ones, as discussed for different context and flow kinematics. When considering a system composed by several DEP with distributed aspect ratio Λ, as for the considered porous system, the overall BTC is given by the previous equation, properly averaged over the distributed τ_D:

$$f(t) = \int_{\Omega} \frac{1}{\Gamma(\frac{1}{3})\,[(\lambda\Lambda)^2/D]^{1/3}} \left(\frac{t}{(\lambda\Lambda)^2/D}\right)^{-2/3} e^{-\frac{t}{(\lambda\Lambda)^2/D}}\, f_{\Lambda}(\Lambda) d\Lambda,$$

where *f(Λ)* is the measured distribution *figure 1 f* and the domain of integration Ω is [1,30]. Without any fitting parameter, the prediction of our model is shown in *figure 2 c* and it fully captures the late time, anomalous, scaling of the measured and simulated BTC.

Given the ubiquity of complex structures in natural (e.g. soil or geologic reservoirs) or industrial (as filtration devices) porous systems, we anticipate that the fundamental mechanisms of coupled advection within vortexes and molecular diffusion, uncovered here for porous media characterized dead-end-pores with distributed aspect ratios, controls the transport of a broad range of colloids and other colloidal-like particles, as bacteria and viruses.